

Modelling parametric uncertainty in PDEs models via Physics-Informed Neural Networks

Milad Panahi · Giovanni Michele Porta ·
Monica Riva · Alberto Guadagnini

Received: August 08, 2024 / Accepted: date

Abstract We provide an approach enabling one to employ physics-informed neural networks (PINNs) for uncertainty quantification. Our approach is applicable to systems where observations are scarce (or even lacking), these being typical situations associated with subsurface water bodies. Our novel physics-informed neural network under uncertainty (PINN-UU) integrates the space-time domain across which processes take place and uncertain parameter spaces within a unique computational domain. PINN-UU is then trained to satisfy the relevant physical principles (e.g., mass conservation) in the defined input domain. We employ a stage training approach via transfer learning to accommodate high-dimensional solution spaces. We demonstrate the effectiveness of PINN-UU in a scenario associated with reactive transport in porous media, showcasing its reliability, efficiency, and applicability to sensitivity analysis. PINN-UU emerges as a promising tool for robust uncertainty quantification, with broad applicability to groundwater systems. As such, it can be considered as a valuable alternative to traditional methods such as multi-realization Monte Carlo simulations based on direct solvers or black-box surrogate models.

Article Highlights

- PINN-UU, a physics informed neural network is introduced to solve PDEs with uncertain physical parameters
- PINN-UU accurately reproduces direct solver results for multiple parameter realizations
- A stage learning approach is employed to overcome convergence failures in the optimization problem

Keywords Physics Informed Neural Networks (PINNs) · Uncertainty Quantification · Sensitivity Analysis · Contaminant Transport

M. Panahi (0000-0002-8776-5297) · G. M. Porta* (0000-0002-0636-373X) · A. Guadagnini (0000-0003-3959-9690) · M. Riva (0000-0002-7304-4114)
Dipartimento di Ingegneria Civile e Ambientale, Politecnico di Milano, Piazza L. da Vinci 32, 20133 Milano, Italy

* Corresponding author E-mail: giovanni.porta@polimi.it

1 Introduction

Groundwater is a critical component of the hydrologic cycle, hydraulic redistribution across the subsurface being a major driver supporting crops, vegetation and surface water bodies (Condon et al., 2021). Having at our disposal effective approaches to groundwater modeling can contribute to expand the boundaries of our knowledge of processes that can govern system dynamics at various scales and ultimately imprint the long-term behavior of hydrogeological scenarios of interest (Bethke, 2022). Due to their inherent simplification of reality (Crawford, 1999), models are typically subject to epistemic and aleatory uncertainty. Key challenges arise in conceptualizing the system behavior and providing an associated mathematical formulation, defining and characterizing input parameters, and addressing the associated uncertainties. The latter element is especially critical for high-dimensional parameter spaces (e.g., Neuman (2003); Tartakovsky (2013); Ceriotti et al. (2018); Psaros et al. (2023) and references therein).

Model parameter estimation is commonly carried out within an inverse problem framework (Carrera and Neuman, 1986). Model calibration can be challenging and costly, particularly when dealing with subsurface systems where measurements are scarce and sparse (in space and time) or (sometimes) not available (Dai and Samper, 2004). To address these challenges, it is important to provide tools that can assist one to prioritize parameters to be estimated during characterization and optimize data acquisition during sampling campaigns (Ceriotti et al., 2018; Janetti et al., 2021). Robust sensitivity analyses (SA) and forward uncertainty quantification (UQ) (Lee and Chen, 2009) techniques are key to achieving these objectives.

In the realm of uncertainty quantification, Monte Carlo (MC) approaches have been broadly employed (e.g., Ballio and Guadagnini (2004); Panzeri et al. (2014) and references therein). These typically rely on multiple evaluations of the system model, each of these corresponding to a randomly sampled set of (uncertain) model input parameters. As such, the ensuing computational cost can be significant, depending on model complexity (in terms of processes included and parametrization). Reduced complexity approaches based on, e.g., analytical and semi-analytical (Pasetto et al., 2014, 2011; He et al., 2011) models, polynomial chaos expansions (Riva et al., 2015; Fajraoui et al., 2011; Janetti et al., 2021) and neural networks (Tang et al., 2020, 2021; Liu and Durlofsky, 2021; Manzoni et al., 2023), are valuable to approximate the behavior of complex groundwater systems while significantly reducing computational costs (Asher et al., 2015). Each of these approaches offers unique advantages and limitations, and their applicability depends on the specific context under analysis.

Deep learning has emerged as a major tool in several fields of research. In this framework, deep neural networks (DNNs) are increasingly employed to tackle classical applied mathematics problems, such as to approximate the solution of partial differential equations (PDEs) (Blechschmidt and Ernst, 2021). This shift in scientific computing is facilitated by the universal approximation capability and high expressivity of neural networks, making them particularly valuable for solving complex PDEs characterized by significant nonlinearities. DNNs are ansatz spaces for the solutions of PDEs (Mishra and Molinaro, 2022) relying on collocating PDEs residual at training points (Cybenko, 1989; Barron, 1993; Kingma et al., 2015). Physics-Informed Neural Networks (PINNs) (Lagaris et al., 1998,

2000; LeCun et al., 2015; Raissi et al., 2019, 2017, 2020) have recently emerged as an approximation technique, by transforming the task of directly discretizing differential operators into an optimization problem focused on minimizing a loss function. PINNs achieve this by integrating the mathematical model depicting the dynamics of the system considered into the neural network architecture and enhancing the loss function with a residual term derived from the governing equation (that are typically formulated upon resting on physical principles, e.g., mass, momentum or energy balances). This residual term serves as a constraining factor, effectively bounding the acceptable solution space. In recent years, there has been an exponential growth in the amount of studies presenting algorithms with PINNs for various applications (e.g., Raissi and Karniadakis (2018); Ray and Hesthaven (2018); Mishra (2018); Lye et al. (2021)). PINNs have also been proposed in the context of groundwater modeling and have shown a remarkable potential in simulating the intricate dynamics of subsurface flow and transport.(e.g., He and Tartakovsky (2021), Shen et al. (2023), Yeung et al. (2022), Tipireddy et al. (2022), and references therein).

In this work we propose a PINN-based method to address epistemic uncertainty associated with unknown physical parameters for sparse-to-none data situations. To address this challenge, we rely on an approach based on a physics-informed neural network under uncertainty (hereafter termed PINN-UU). The concept underlying the method rests on the definition of the computational domain where the problem solution is sought as comprising both (a) the spatiotemporal domain and (b) the space of uncertain parameters. In this sense, our method is inspired to intrusive UQ methods, where the solution accounts directly for stochastic variables (e.g., uncertain parameters (Le Maître and Knio, 2010)). While traditional intrusive UQ methods require major changes in problem formulation and algorithms (Turnquist and Owkes (2019)), PINN-UU offers a framework to streamline the solution strategy. Our approach is not geared to parameter estimation, but rather to exploring the impact of parametric uncertainty onto the system outputs. Thus, we solely rely on the constraints of the physics embedded in the governing equations for solving PDEs (in the form of residual training), as opposed to approaches that combine physical laws and scattered (noisy) measurements for learning stochastic processes and addressing uncertainty quantification (e.g. MH-PINNs (Zou and Karniadakis, 2023), and B-PINNs (Yang et al., 2021)). To this end, we introduce a methodology to fine-tune the neural network-based solution ansatz via transfer learning. In the specific numerical examples discussed here our objective is to harness the capabilities of PINNs to provide an efficient and accurate tool for UQ in predicting solute transport in porous media. We thus showcase the application of PINN-UU to the solution of a scenario associated with solute transport in the presence of adsorption.

The study is organized as follows. In Section 2 we provide the overall formulation of our new abstract PDE setting and describe briefly vanilla PINNs as the base PDE solver for our new problem set. PINN-UU is described in Section 3. Section 4 focuses on the results of its application to an exemplary scenario associated with solute transport in the presence of sorption in a porous medium and on a comparison against an approach to the solution of the PDE governing the process analyzed through a typical finite difference method (FDM). We then analyze the applicability of PINN-UU within a global sensitivity analysis framework.

(a)	
1) Forward stochastic	Property
$\mathcal{F}_{x,\lambda}, \mathcal{B}_{x,\lambda}$	known
$f_\lambda(\mathbf{x}), b_\lambda(\mathbf{x})$	known
$u(\mathbf{x}; \boldsymbol{\lambda})$	unknown
$\boldsymbol{\lambda}$	stochastic
Objective	find $u(\mathbf{x}; \boldsymbol{\lambda})$ for $\forall \mathbf{x} \in \Omega_\lambda$

(b)	
2) Forward deterministic	Property
$\mathcal{F}_x, \mathcal{B}_x$	known
$f(\mathbf{x}), b(\mathbf{x})$	known
$u(\mathbf{x})$	unknown
$\boldsymbol{\lambda}$	deterministic
Objective	find $u(\mathbf{x})$ for $\forall \mathbf{x} \in \Omega$

Table 1: The (a) forward stochastic scenario properties addressed in this work compared against the classical (b) forward deterministic scenario.

2 Methodology

2.1 Problem formulation

Consider the following partial differential equation (PDE) describing the space-time dynamics of the state variable, $u(\mathbf{x}; \boldsymbol{\lambda})$, of a physical system

$$\mathcal{F}_{x,\lambda}[u(\mathbf{x}; \boldsymbol{\lambda})] = f(\mathbf{x}; \boldsymbol{\lambda}) \quad \mathbf{x} \in \Omega, \quad (1)$$

where \mathbf{x} denotes the D_x -dimensional **space-time** coordinate, $\boldsymbol{\lambda} \in \Lambda \subseteq \mathbb{R}^{N_\lambda}$ represents a vector of (generally unknown) physical/model parameters, $\mathcal{F}_{x,\lambda}$ (hereafter referred to as F_λ for brevity of notation) denotes the differential operator and $f(\mathbf{x}; \boldsymbol{\lambda})$ (hereafter referred to as f_λ) is the forcing function. Equation(1) is subject to the following boundary/initial conditions

$$\mathcal{B}_{x,\lambda}[u(\mathbf{x}; \boldsymbol{\lambda})] = b(\mathbf{x}; \boldsymbol{\lambda}) \quad \mathbf{x} \in \Gamma, \quad (1a)$$

where $\mathcal{B}_{x,\lambda}$ (hereafter referred to as B_λ) denotes the boundary/initial operators and $b(\mathbf{x}; \boldsymbol{\lambda})$ (hereafter referred to as b_λ) is the boundary/initial function.

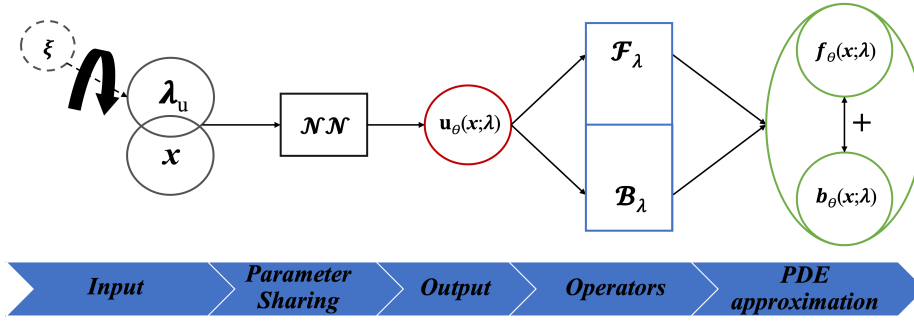


Fig. 1: PINN-UU architecture. Here, ξ denotes a random number generator associated with a desired distribution (e.g., uniform) and employed to sample training points in the Ω_λ space.

Physical parameters are included in vector $\boldsymbol{\lambda} = [\boldsymbol{\lambda}_k, \boldsymbol{\lambda}_u]$. The latter is formed by N_{λ_k} deterministic ($\boldsymbol{\lambda}_k$) and N_{λ_u} uncertain ($\boldsymbol{\lambda}_u$) parameters. We consider all entries of $\boldsymbol{\lambda}_u$ to be multivariate uniform stochastic variables, i.e., $\boldsymbol{\lambda}_u \sim \mathcal{U}(\boldsymbol{\lambda}_{u,min}, \boldsymbol{\lambda}_{u,max})$, where $\boldsymbol{\lambda}_{u,min}$, $\boldsymbol{\lambda}_{u,max}$ represent lower and upper bounds of the parameter supports, respectively. The parameter space Λ identifies the domain considering all possible parameters combinations. We introduce the problem domain $\Omega_\lambda = \Lambda \times \Omega$, and $\Gamma_\lambda = \Lambda \times \Gamma$ by jointly considering the spatiotemporal domain (Ω) and domain boundary Γ together with the parameter support space (Λ). Thus, the dimension of Ω_λ corresponds to $N_{\bar{p}} = D_x + N_{\lambda_u}$. Our objective is to obtain the solution $u(\mathbf{x}; \boldsymbol{\lambda})$ at every $(\mathbf{x}; \boldsymbol{\lambda}) \in \Omega_\lambda$.

Following Psaros et al. (2023), we classify problem sets as neural PDEs when we have complete knowledge of the operators F_λ and B_λ . In this context, the distinctive element of neural PDEs used in our work is their dependence on neural networks (NNs) as a central computational framework. Our methodological workflow is then characterized by the key features listed in Table 1a and pertains to a *forward stochastic* PDE problem (i.e., F_λ and B_λ are stochastic) as opposed to conventional *forward deterministic* PDEs, where F_λ and B_λ are deterministic (see Table 1b).

3 Physics Informed Neural Network Under Uncertainty (PINN-UU)

In the following we describe the **PINN Under Uncertainty (PINN-UU)**. Our approach is built on classical PINNs. A schematic depiction of our PINN-UU is shown in Fig. 1. The dependency of the network parameters on the uncertain (stochastic) parameters $\lambda_u \in \boldsymbol{\lambda}$ is fully taken into account, as our network receives the PDE parameter values in the input stage.

The PINN-UU network comprises an input layer that incorporates the parameter values, followed by multiple shared hidden layers with dropout regularization, and an output layer for the PDE unknown solution. Similar to PINNs, our neural network is also trained using a combined loss function that includes the residual of the PDE equations and the boundary/initial conditions. In the context of

Algorithm 1 Training PINN-UU

Inputs:

- i. Multi-dimensional domain Ω_λ
- ii. differential operator \mathcal{F}_λ , boundary/initial operator \mathcal{B}_λ and their corresponding source terms f_λ and b_λ for PDE (1)

Goal: Find PINN-UU solution $u^* = u_{\theta_\lambda^*}$ for approximating PDE (1).

Step 1: Construct the neural network u_θ architecture, specifying the input dimension as $N_{\bar{p}} = D_x + N_{\lambda_u}$

Step 2: $k \leftarrow N_{\lambda_u}$, assign N_{λ_u} to the iterator index k , and initialize the neural network parameter vector $\bar{\theta}_\lambda^k$ using Xavier Glorot's initialization.

while $k \geq 0$ **do**

Step 3: Set the first k entries of $\{\lambda_u^i\}_{i=1}^k$ equal to the **mean** of their corresponding **probability distribution**, and sample the remaining $N_{\lambda_u} - k$ members, from their corresponding **probability distribution**.

Step 4: For the initialized value of the network parameter vector $\bar{\theta}_\lambda^k$, run an optimization algorithm of choice until an approximate local minimum θ_λ^{k*} of Eq. (3) is reached.

Step 5: $\bar{\theta}_\lambda^{k-1} \leftarrow \theta_\lambda^{k*}$, i.e., we transfer the learned parameters of previous stage θ_λ^{k*} and use it to initialize the neural parameters $\bar{\theta}_\lambda^{k-1}$ for the next step ($k-1$)

Step 6: $k \leftarrow k - 1$ iterate over while loop, i.e., decrease the iterator index by one

end while

Step 7: The map $u^* = u_{\theta_\lambda^{k*}}|_{k=0}$ is the desired PINN-UU for the approximation of the solution $u(\mathbf{x}; \lambda)$ of PDE (1)

our framework, the optimization problem to find neural networks u_{θ_λ} with tuning parameters θ_λ can be rewritten as:

$$\hat{\theta}_\lambda = \underset{\theta_\lambda}{\operatorname{argmin}} \mathcal{L}(\theta_\lambda), \quad \mathcal{L}(\theta_\lambda) := \int_{\Omega_\lambda} |\mathcal{F}_\lambda(u_{\theta_\lambda}) - f_\lambda|^2 dx + \int_{\Gamma_\lambda} |\mathcal{B}_\lambda(u_{\theta_\lambda}) - b_\lambda|^2 dx, \quad (2)$$

knowing that PDE (1) must hold for any $\mathbf{x} \in \Omega_\lambda, \Gamma_\lambda$. The training set (of size N_f) for the interior domain will include (a) $N_{\bar{P}}$ -tuplets of residual training points in Ω_λ and (b) the training set of size N_b and N_0 for the spatial boundary and initial conditions, respectively. The training strategy is presented in Algorithm 1 and described in details in Section 3.1. The neural network architecture is fixed throughout the training.

The minimization problem in Eq. (3) amounts to finding a minimum of a possibly non-convex function over a high-dimensional space. We solve this minimization problem with a first-order stochastic gradient descent, ADAM (Kingma and Ba, 2014), followed by a higher-order optimization method, LBFGS (Liu and Nocedal, 1989). Following determination of θ_λ as our best approximate/local minimum, the underlying network u_θ can be evaluated at any $\mathbf{x} \in \Omega_\lambda$ as our PINN approximation for the solution u of PDE (1).

3.1 Transfer learning (Warm-starting)

The neural network parameter space grows with the dimension of problem sampling space (Ω_λ). This leads to a corresponding increase of computational complexity and memory requirements. This issue hampers the efficient training of PINNs and often results in slow convergence rate and increased likelihood of trapping in local minima. Introducing the PDE parameters as inputs to the PINNs has two main drawbacks: a) dealing with high-dimensional space leads to computational issues in the training phase; and b) the level of complexity of the loss surface increases, thus causing network optimization to fail or to require unaffordable computational resources. In order to alleviate these negative aspects, we rely on a broadly known technique termed transfer learning. Here, we train our PINN-UU via a stage learning strategy, where we initiate the training process by employing parameters retained from prior sessions (see Algorithm 1, steps 3 to 5), stored in memory, thereby adopting a *warm-start* strategy. This is in contrast with the *cold-start* approach, where training begins with entirely random parameters (Raissi, 2023). Doing so can speed up convergence of the optimization problem and minimizes the probability of being trapped in local minima. We start from lower dimensions (i.e., corresponding to the classic spatiotemporal domain with fixed parameter values as inputs) and use the trained network parameters as a first guess candidate to initialize training on higher dimensions as we introduce stochastic parameters one by one to the sampling space. In the first iteration all parameters in λ are considered deterministic and fixed to the mean value of their corresponding probability density function. We then introduce one stochastic parameter at each step according to the while loop shown in Algorithm 1). In other words, parameters are initially fixed to their mean value and then progressively sampled from their corresponding distributions. According to Mishra and Molinaro (2023), our network generalization error can be upper-bounded and determined by training error and number of residual training points. Therefore, this network can (in principle) be a viable candidate as a neural solver to address our new problem formulation.

4 Results and Discussion

4.1 Problem formulation

In this section we illustrate the results of numerical experiments aimed at examining the performance of the proposed PINN-UU. We investigate solute transport coupled with sorption in porous media. This is modeled upon relying on the Advection-Dispersion Equation (ADE) and including a retardation factor that is represented through the Langmuir sorption isotherm (Fetter et al., 1999).

After describing the PDE formulation and the parameter settings in Section 4.1.1, Section 4.1.2 summarizes the outcomes of our systematic exploration aimed at identifying the optimal network configuration. We then present in Section 4.2 a comparison between the performance of PINN-UU and a reference Finite Difference Method (FDM). We consider an instance-wise (Section 4.2.1) level of comparison and a comparison based on the probability density function of model outputs (Section 4.2.2). For the latter analysis, we rely on a large dataset comprising 10^6 Monte Carlo realizations of the uncertain parameters λ_u and their corresponding PDE solution for PINN-UU and FDM, denoted in the following as u_{pre} and u_{ref} , respectively. Finally, in Section 4.3 we illustrate the way PINN-UU can be employed in the context of global/local sensitivity analysis.

4.1.1 Governing Equation

The one-dimensional advection-dispersion equation coupled with Langmuir sorption isotherm can be expressed as:

$$\begin{cases} u_t \left[1 + \frac{\rho_b}{\theta} \left(\frac{K_l Q}{(1 + K_l u^2)} \right) \right] - (Du_{xx} - vu_x) = 0 & x \in \Omega; \lambda_u = [D, K_l, Q] \\ vu - Du_x = Q_{in} & x \in \partial\Omega_F \\ u_x = g_N & x \in \partial\Omega_N \\ u = u_0 & x \in \partial\Omega_0, \end{cases} \quad (3)$$

where u denotes concentration of the solute in the liquid phase in the spatiotemporal domain Ω ; $\mathbf{x} = (x, t)$ is space-time coordinate vector; ρ_b and θ are bulk density and porosity of the porous medium, respectively; K_l is the Langmuir adsorption constant (or adsorption rate); Q is the maximum amount of solute that can be adsorbed per unit of solid surface (hereafter termed as maximum adsorption); D is dispersion coefficient, embedding molecular diffusion and hydrodynamic dispersion; v is the average pore velocity; g_N is prescribed mass flux at the effluent boundary $\partial\Omega_N$; Q_{in} is the solute mass flux imposed at the inlet boundary $\partial\Omega_F$; and u_0 is the initial condition for concentration, Ω_0 denoting initial time.

Table 2 lists the parameter values/ranges that we employ to solve Eq. (3) for the entire 5-dimensional space Ω_λ . Our problem set mimics a continuous injection of a solute in a homogeneous porous domain where the initial concentration is set to zero and closely resembles conditions in column flow-through experiments.

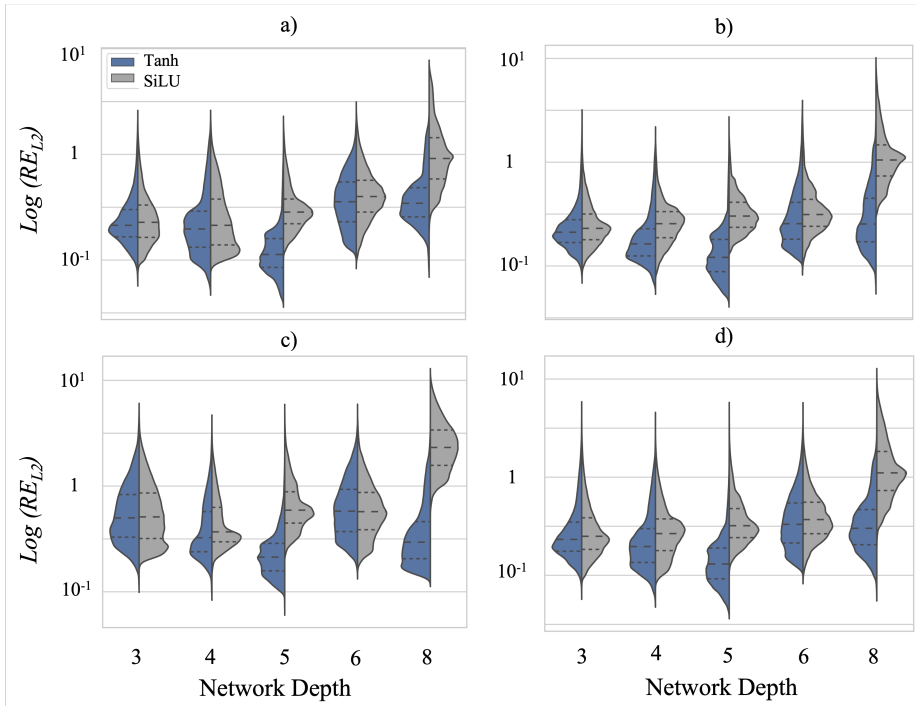


Fig. 2: Model tuning: distribution of the relative percentage errors RE_{L2} (Eq. (4)) between the reference FDM solution and the examined PINN-UU architectures. Shaded areas with different colors, blue and grey, correspond to the two activation functions employed, i.e., Tanh and SiLU, respectively. Results are shown for three different regimes corresponding to a) low, b) medium, and c) high Péclet, as well as d) overall. Dashed lines correspond to the first, second, and third quartiles. The loosely dashed line and the densely dashed lines represent the median, and (25^{th} , 75^{th}) percentiles, respectively.

Each uncertain parameter is characterized by a uniform probability density function. The widths of the corresponding supports correspond to about an order of magnitude (in terms of parameter values) and are designed to include ranges of parameter values commonly employed and discussed in the literature. The Péclet number, Pe , resulting from our selected interval spans the range (10,100), thus considering transition from mild to strongly advection-dominated conditions.

Average values of parameters K_l and Q are selected to yield a retardation factor approximately equal to 2 when considering the reference concentration $u = Q_{in}/v = 1$.

4.1.2 Neural Network Architecture and Training Procedure

We employ neural networks with diverse architectures to assess their ability to provide accurate solutions of Eq. (1). The input layer comprises 5 neurons (corre-

Parameter	Ranges/Values	Variable Type
$(x[L], t[T])$ or \mathbf{x}	$[0, X = 30] \times [0, T = 15]$	λ_u
λ_1 or $D[L^2T^{-1}]$	(3, 30)	
λ_2 or $K_l[L^3M^{-1}]$	(0.01, 0.1)	
λ_3 or $Q[MM^{-1}]$	(1, 10)	
$Pe[-] = \frac{X \times v}{D} = \frac{30 \times 10}{D}$	(10, 100) $Pe < 15 \Rightarrow$ Low $15 \leq Pe \leq 40 \Rightarrow$ Med $Pe > 40 \Rightarrow$ High	-
$\rho_b[MM^{-3}]$	1.6	λ_k
$\theta[-]$	0.37	
$v[LT^{-1}]$	10	
$Q_{in}[ML^{-2}T^{-1}]$	10	
$g_N[ML^{-1}]$	0	
$u_0[ML^{-3}]$	0	

Table 2: Description of problem setting. Training points are samples from (\mathbf{x}, λ_u) across our 5 – dimensional space Ω_{λ_u} . Parameters $[D, K_l, Q]$ are categorized as uncertain, while the remaining parameters are fixed (i.e., are of λ_k -type).

Step ID ($N_{\lambda_u} - k$)	Ω_{λ}	$[N_f, N_b, N_0]$
0	$x \times t \times \bar{D} \times \bar{K}_l \times \bar{Q}$	$[10k, 50, 50]$
1	$x \times t \times D \times \bar{K}_l \times \bar{Q}$	$[200k, 5k, 5k]$
2	$x \times t \times D \times K_l \times \bar{Q}$	$[1000k, 50k, 50k]$
3	$x \times t \times D \times K_l \times Q$	$[3000k, 100k, 100k]$

Table 3: Training points sampling scheme; k corresponds to $\times 10^3$; overbar symbols $\bar{\cdot}$ indicate parameters that are sampled equal to their corresponding distribution average value in each training iteration, as cited in Algorithm 1.

sponding to our 5 – dimensional space Ω_{λ}) to sample the residual training points. We then systematically vary the network depth (i.e., the number of hidden layers) and width (i.e., the number of neurons in each layer), to appraise different levels of complexity within the PDE solution space. Each of these configurations is associated with two activation functions, namely hyperbolic Tangent (Tanh) and Scaled Exponential Linear Unit (SiLU; also known as Swish). These activation functions are selected to introduce non-linearity into the network. The explored architectures include configurations with [depth, width] of [3, 250], [4, 220], [5, 150], [6, 50], and [8, 100]. Therefore, we explore a total of 10 distinct network architectures.

Transport Regime	Best Performance	Worst Performance
Low Pe	[0.038, 13, 0.067, 3.78]	[1.23, 10, 0.1, 1]
Med Pe	[0.043, 18, 0.03, 1.64]	[1.64, 37, 0.01, 10]
High Pe	[0.065, 43, 0.034, 1.4]	[2.12, 79, 0.01, 10]

Table 4: Combinations of the transport model unknown parameters with their corresponding RE_{L2} (Eq. (4)) value for best and worst performance associated with the three distinct transport regimes, corresponding to low, medium, and high Péclet value. Values inside brackets correspond to $[RE_{L2}, Pe, K_l, Q]$.

To enhance the network resilience and generalization ability, we add dropout layers with a dropout rate of 0.5 after each hidden layer. Adoption of, (a) Glorot normal initialization (Glorot and Bengio, 2010) for the network weight parameters, and (b) Soft Attention Mechanism (SAM) refined through adversarial learning strategy (McClenney and Braga-Neto, 2020), contributes to achieve stable training and to force the neural network to fit better stubborn spots (where the solution space includes regions with rapid variation due to stiffness) in the solution of our PDE, respectively. We also use mini-batch learning for PDE residual training points (N_f) to alleviate computational costs of large matrix multiplications, while keeping full-batch learning for initial and boundary residual training points (N_0 and N_b , respectively).

The training procedure is implemented in Tensorflow 2.10 for 100k, 50k, and 10k iterations of ADAM for $N_{\lambda_u} = 3$ steps of our multi stage training, consistent with the number of uncertain physical parameters (D, K_l, Q). This is then followed by 1k iterations of L-BFGS quasi-newton method in some cases to fine tune the network weights. The number of residual training points selected for the trials is also listed in Table 3. We rely on the Sobol sampling strategy to optimize placement of training points across the domain.

Training is implemented on a single Nvidia GeForce RTX 4090 GPU. We implement SAM and apply locally (i.e., per training point) adaptive loss weights initialized to be 1. The exponentially decaying learning rates for network trainable parameters and self-adaptive weights are initialized at 4e-3 and 2e-3, respectively, with decay steps of 5% of the total training iterations.

Figure 2 depicts (sample) probability density functions (PDFs) of L2-Norm relative error percentages RE_{L2} , evaluated as:

$$RE_{L2} = 100 \times \frac{\|u_{pre} - u_{ref}\|_2}{\|u_{ref}\|_2} \quad [\%], \quad (4)$$

The PDFs shown in Figure 2 are evaluated considering a Monte Carlo sample of 10^6 realizations. it can be noted that similar PDFs of RE_{L2} are obtained in all of the tested network configurations. Nevertheless, our results indicate that, in general, a network architecture featuring a depth of 5 hidden layers and a width of 150 neurons, trained with the Tanh activation function exhibits a slightly better performance (due to lower mean relative error and more precision) than the other configurations. In scenarios characterized by high Péclet numbers, leading to

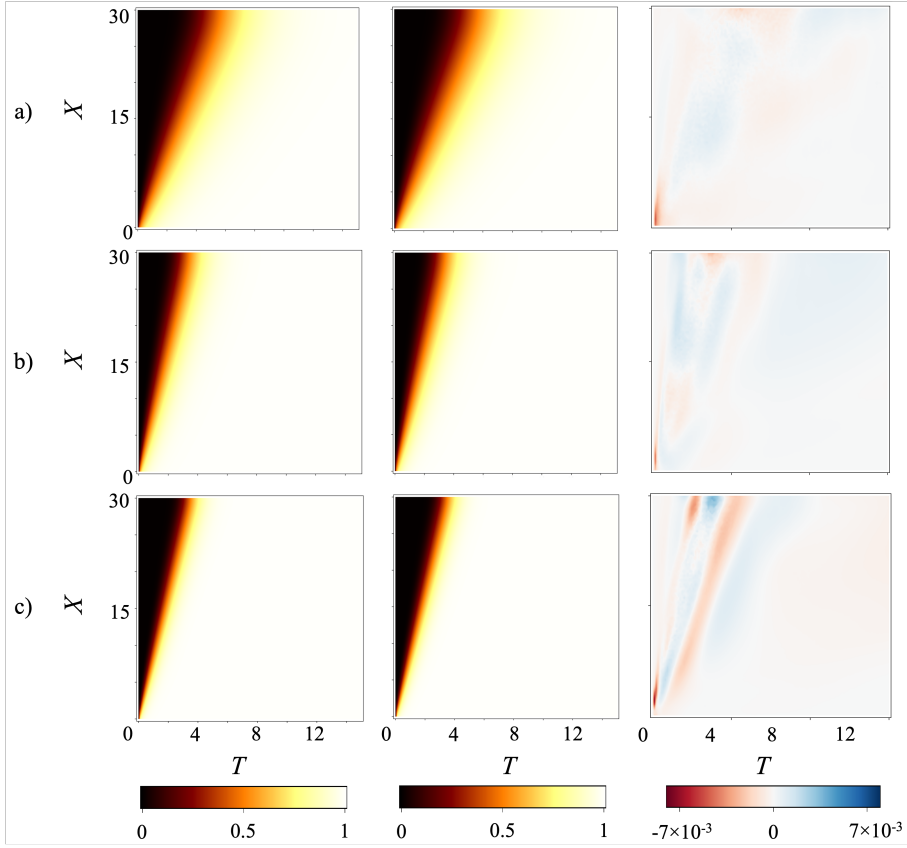


Fig. 3: Space-time distribution of the results of the best performing PINN-UU, u_{pre} (1st column), reference Finite Difference solution, u_{ref} (2nd column), and their corresponding point-wise error [$u_{pre} - u_{ref}$] (3rd column), for a) low, b) medium, and c) high Péclet.

steep solution surfaces, the network [5, 150] gives a performance similar to the high complexity network architecture with the deepest configuration, corresponding to network [8, 100]. We also observe a noteworthy distinction in the performance of the SiLU activation function when compared to Tanh, particularly in the context of deeper networks. On average, the SiLU activation function exhibits a slightly inferior performance, a phenomenon that may be attributed to challenges associated with vanishing gradients (Nwankpa et al., 2018).

Based on our findings, selecting a moderately-deep PINN-UU, i.e., [5, 150] as the most performant model yields accurate results within an acceptable computational time-frame of approximately 5 GPU-Hours for the test case considered.

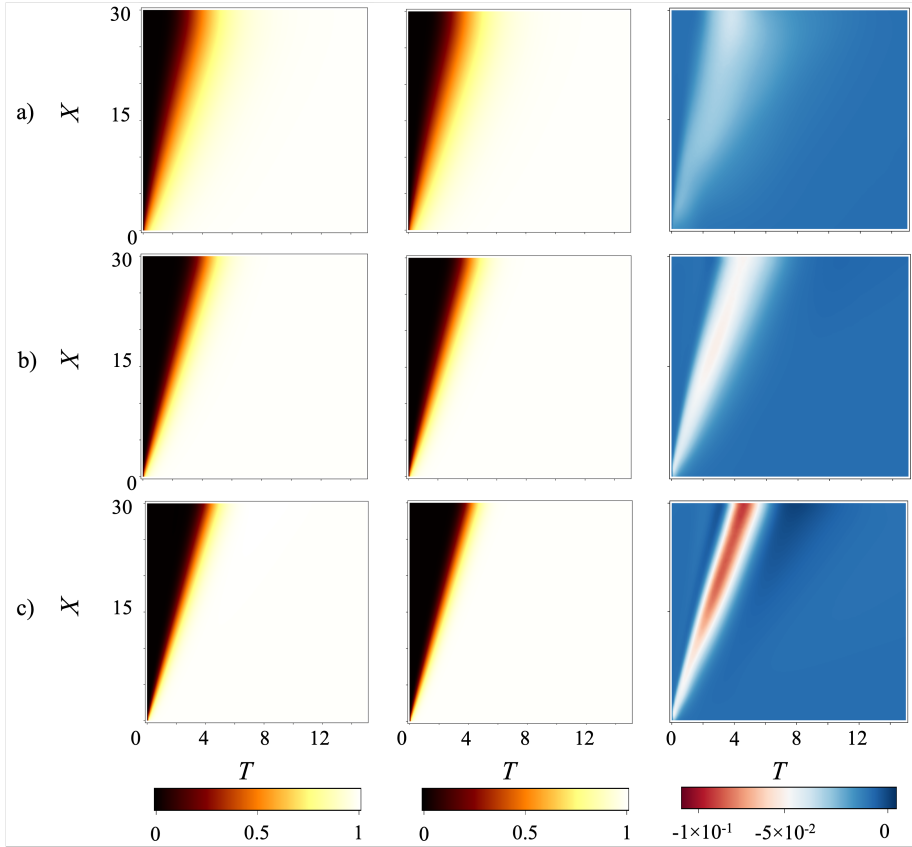


Fig. 4: Space-time distribution of the results of the worst performing PINN-UU (1st column), to reference Finite Difference solution (2nd column), and their corresponding point-wise error (3rd column) for a) low, b) medium, and c) high Péclet.

4.2 Error Analysis

In this section, we perform a comprehensive analysis of the performance of the selected neural network model configuration (i.e., [5, 150]). We consider the results of individual realizations (Section 4.2.1) and an analysis of the ensuing probability density functions (Section 4.2.2).

4.2.1 Instance Wise Analysis

We perform here pairwise comparisons between the results obtained through PINN-UU and the reference solution (FDM) for selected parameter realizations. Figure 3 and Figure 4 respectively illustrate the best- and worst-performing model realizations generated by PINN-UU (here denoted as u_{pre}) alongside the reference solutions (here denoted as u_{ref}) for three distinct transport regimes (low, medium, and high Péclet) as well as the space-time distribution of the related point-wise

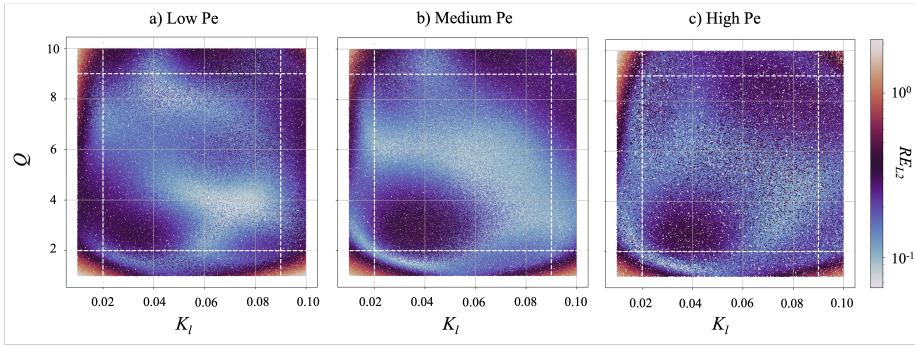


Fig. 5: PINN-UU blind spots. Relative percentage errors RE_{L2} (Eq. (4)) between the reference FDM solution and the examined PINN-UU architectures in the K_l and Q parameter space. Results are evaluated on the basis of 10^6 Monte Carlo parameter combination samples and correspond to a) Low, b) Medium, and c) High Péclet.

errors (calculated as $(u_{pre} - u_{ref})$). The associated RE_{L2} value and parameter values related to best and worst performance are included in Table 4.

Our results show that the largest point-wise errors are of the order of 0.1% (for the best-performing realizations) and 10% (for the worst-performing realizations). The regions around steep gradients are characterized by the largest errors. The latter are generally observed for large Pe (advection-dominated conditions), where gradients become sharper.

Notably, in the worst-performing case (Fig. 5) PINN-UU only slightly underestimates the reference solution in steep regions (advection fronts). When considering the impact of parameter values on model performance (see Table 4), we observe that the worst-performing models are overall associated with K_l and Q values close to the boundary of their corresponding intervals. This suggests that low accuracy regions (here termed blind spots) may exist near the boundaries of the parameter space λ_u . Figure 5 confirms the existence of these blind spots, depicting the distribution of RE_{L2} with regards to parameters K_l and Q .

As stated in Section 4.1.2, training points are selected through Sobol sampling, a quasi-Monte Carlo technique, which is employed to efficiently sample the vast parameter space (Ω_λ) of our problem formulation. We recall that the distribution of samples ensuing the application of Sobol sampling can still be influenced by various factors, including the dimensionality of the parameter space and the specific characteristics of the problem. The so-called blind spots can be attributed to both the boundary effects, where system behavior can change significantly near parameter boundaries, and the aforementioned under-sampling issue. The latter arises because the distribution of samples may not adequately capture the complexities of these critical regions. As such, while our model demonstrates a good performance in well-sampled areas, its accuracy diminishes near parameter boundaries, likely due to the limited sample density available for training. Note also that, as opposed to the physical time-space domain, no boundary condition can be assigned along the λ_u of the domain Ω_λ , this factor possibly contributing to the observed accuracy loss. Understanding these limitations is critical for interpreting the reliability

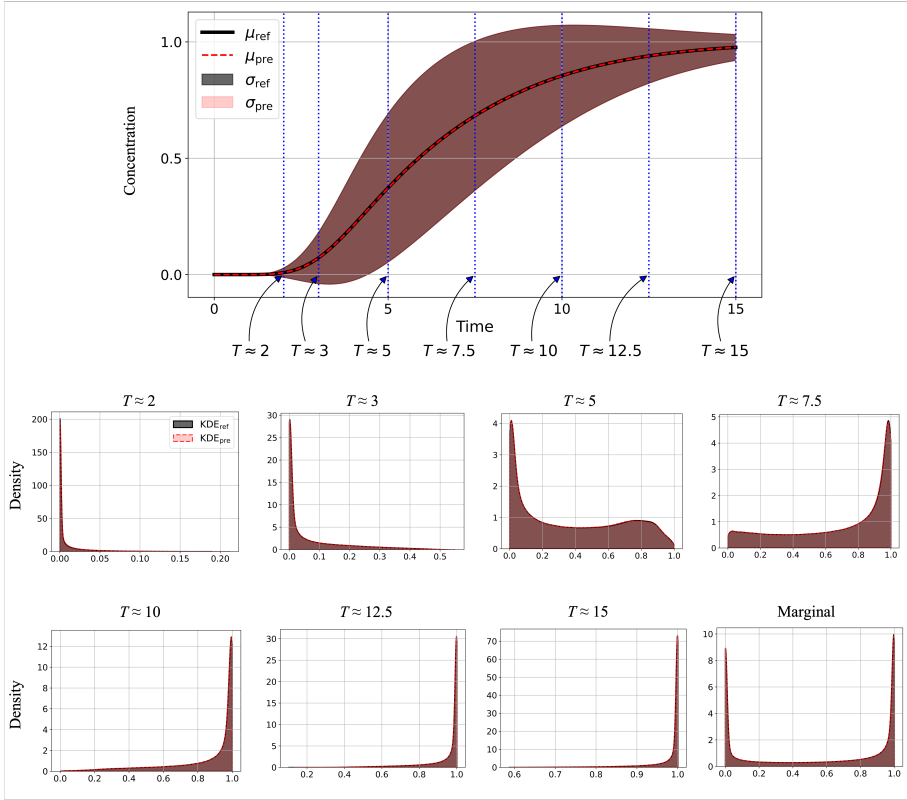


Fig. 6: Statistical analysis of solute breakthrough curves (BTCs) samples. The upper panel shows the mean (red dashed and black solid curves) and the standard deviation (red and black combined shadowed areas) of the temporal evolution of effluent concentration (u_e) obtained through 10^6 Monte Carlo samples from the parameter space generated by our PINN-UU compared to reference numerical solver (FDM). The remaining panels illustrate sample PDFs of effluent concentrations conditional on selected time (as indicated by black arrows in the first panel). The marginal (with respect to time) probability distribution of the effluent concentration, representing the probability density of attaining a given outlet concentration value independent of time, is also depicted. Note that the shaded areas with diverse colors essentially overlap in all panels.

of PINN-UU results in scenarios that approach the boundaries of the parameter space. To mitigate this challenge, future investigations may consider augmenting sampling density near boundaries or exploring alternative sampling strategies to enhance model performance across the entire parameter space.

4.2.2 Statistical Analysis of Model Outputs

To gain further insights into the predictive capabilities of our PINN-UU framework, in Figure 6 we juxtapose the temporal evolution of mean (μ) and standard

deviation (σ) of the effluent concentrations, u_e , computed on the bases of 10^6 Monte Carlo simulation using PINN-UU (μ_{pre} and σ_{pre} , the corresponding mean and standard deviation, respectively) and FDM (μ_{ref} and σ_{ref} , the corresponding mean and standard deviation, respectively). Note that the FDM model requires performing a complete simulation for each sampling point. Otherwise, once our PINN-UU is trained, it produces the results on-demand post-training. Figure 6 also includes a Kernel Density Estimations (KDE) of the probability density functions of effluent concentrations at selected times (i.e., the PDF conditional to time). The marginal (with respect to time) probability distribution of the effluent concentration, representing the probability density of attaining a given outlet concentration value independent of time, is also depicted. Note that time level $T = 3$ corresponds to one pore volume, i.e., the median solute arrival time that would be attained without sorption.

At all times, the first two moments of the concentration as wells as concentration PDFs obtained with PINN-UU essentially overlap with those obtained via FDM. This analysis substantiates the PINN-UU accuracy and provides insights into its ability to capture the underlying uncertainty in the parameter space. Furthermore, we observe that the PDFs of effluent concentration are heavily skewed, shifting from right- to a left-skewed distributions as time increases. These results demonstrate the ability of PINN-UU to provide an accurate propagation of uniform input distributions (of parameters) onto otherwise non-uniform and asymmetric PDFs of solute concentrations.

4.3 Sensitivity Analysis (SA)

Here, we assess the applicability of our PINN-UU model in the context of sensitivity analysis. Typically, Global Sensitivity Analysis (GSA) and Local Sensitivity Analysis (LSA) frameworks require multiple model realizations. PINN-UU infers on-demand the required sensitivity indices through simple and inexpensive post-processing steps. Figure 7 provides examples of the types of PINN-UU inferences one can obtain documenting the variability of the effluent solute concentration u_e across the support of two parameters (i.e., $[D, K_l, Q]$), the remaining parameters remaining fixed. In the following sections, we explicitly explore the applicability of our model in the contexts of GSA (Section 4.3.1) and LSA (Section 4.3.2). Our Sensitivity Analysis (SA) starts by considering the performance of the transport system as rendered through our target quantity, i.e., solute concentration at the system outlet (u_e).

4.3.1 Global Sensitivity Analysis

Our PINN-UU model is characterized by a clear potential for comprehensive parameter space exploration in the context of global sensitivity analyses. Our exemplary analyses consider three typically used global sensitivity metrics, i.e., the variance-based Sobol indices (Sobol, 1993) and the moment-based AMA indices (Dell’Oca et al., 2017). The principal Sobol index represents the relative expected reduction of process variance due to knowledge of (or conditioning on) a model parameter as:

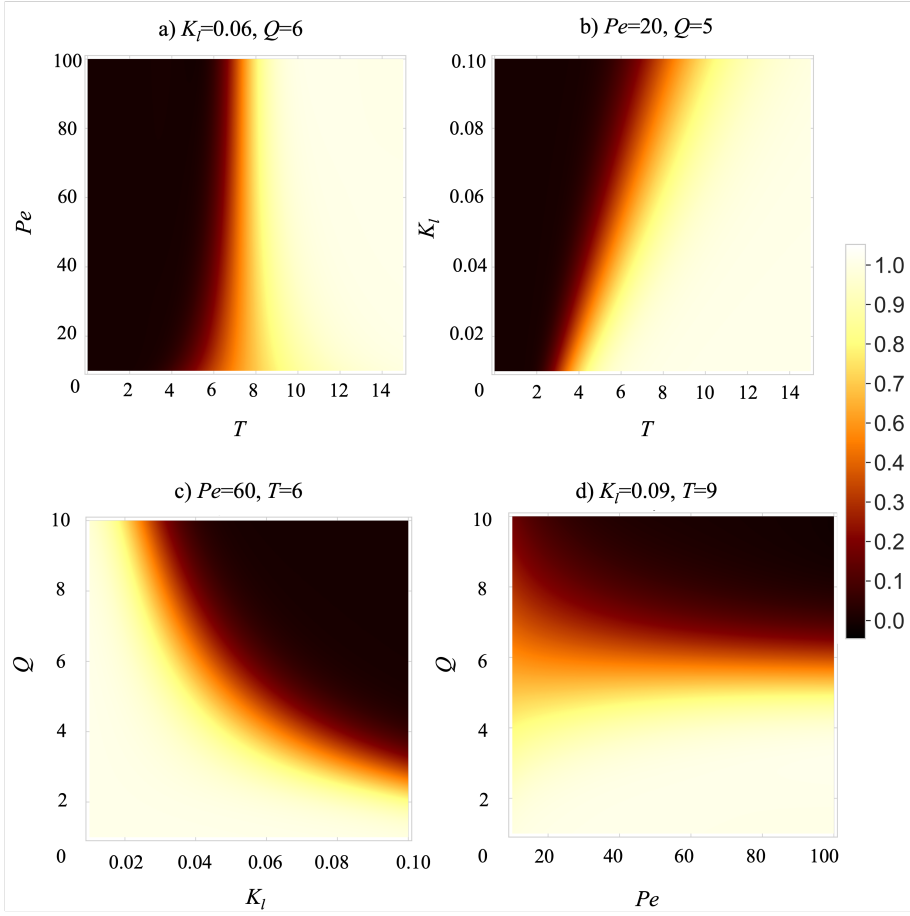


Fig. 7: Impact of different combinations of time, T , and $[D, K_l, Q]$ on solute concentrations at the system outlet.

$$SI_{\lambda_i} = \frac{V[E[u_e | \lambda_i]]}{V[u_e]} = \frac{[V[u_e] - E[V[u_e | \lambda_i]]]}{V[u_e]}, \quad (5)$$

where $E[.]$ and $V[.]$ refer to expected value and variance, respectively.

Dell’Oca et al. (2017) propose GSA metrics (termed AMA indices) based on the first four (statistical) moments of the PDF of target model outputs. This technique provides enhanced information content to enrich the commonly used variance-based GSA (Sobol’, 1993), because uncertainty and sensitivity are characterized by investigating multiple (statistical) moments of the probability density function of the model outputs, rather than being confined to the variance only. For the purpose of our exemplary study, we consider GSA as rendered through the assessment of

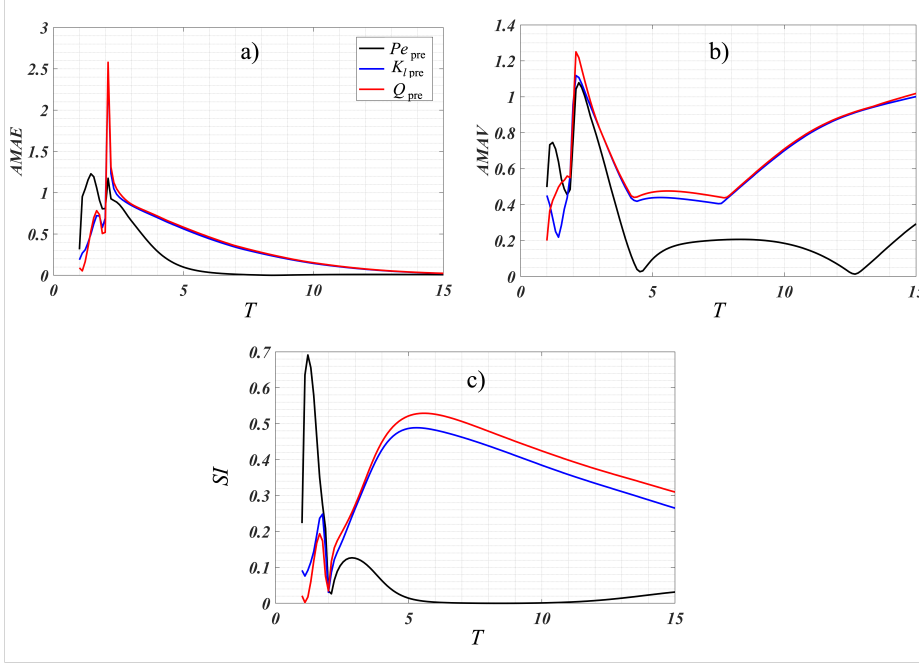


Fig. 8: Temporal distributions of the 3 global sensitivity indices considered for solute concentrations at the system outlet (u_e), i.e., a) $AMAE$, b) $AMAV$, and c) principal Sobol Indices (SI) for three model parameters (Péclet number (Pe) in black; Adsorption rate (K_I) in blue; and Maximum adsorption (Q) in red).

the following AMA metrics:

$$AMAE_{\lambda_i}^{u_e} = \begin{cases} \frac{1}{|E[u_e]|} E[|E[u_e] - E[u_e | \lambda_i]|], & \text{if } E[u_e] \neq 0 \\ E[|E[u_e | \lambda_i]|], & \text{if } E[u_e] = 0 \end{cases} \quad (6)$$

$$AMAV_{\lambda_i}^{u_e} = \frac{E[|V[u_e] - V[u_e | \lambda_i]|]}{V[u_e]}, \quad (7)$$

Here, $AMAE_{\lambda_i}^{u_e}$ and $AMAV_{\lambda_i}^{u_e}$ represent the sensitivity indices associated with the first (mean) and second (variance) moments of u_e , respectively, as linked to variability of λ_i ; the symbol $u_e | \lambda_i$ indicates conditioning of u_e to a known value of λ_i within Λ_{λ_i} . Indices $AMAE_{\lambda_i}^{u_e}$ and $AMAV_{\lambda_i}^{u_e}$ respectively quantify the expected change of the mean and variance of u_e due to our knowledge of λ_i .

Figure 8 depicts the temporal evolution of the three GSA indices described above with respect to all uncertain model parameters. We note some oscillations in the values of the $AMAE$ and $AMAV$ indices at early times. These could be related to the behavior of the PINN-UU near the outlet boundary region during the initial time steps. Concentration attains values very close to zero in these early stages, thus reflecting the influence of the initial condition. We observe that the parameters related to the sorption model have higher influence on the solution

than the dispersion coefficient (here embedded in Pe), particularly for $T > 3$. The indices related to the two parameters K_l and Q essentially overlap. We also observe that index $AMAV$ reveals mild sensitivity of u_e to Pe for $T > 5$, an effect that is not captured through S_i . Otherwise, the value of Pe does not impact the average value of u_e for $T > 5$ (as seen by the virtually zero values for $AMAE$ in Fig. 8). Having at our disposal this kind of information can be critical when diagnosing a model behavior through sensitivity analysis and to assess parameter identifiability and estimation in an inverse modeling framework. The PINN-UU formulation enables extensive sampling at low computational cost, which is a key requirement to efficiently estimate sensitivity indices for high-order moments.

4.3.2 Local Sensitivity Analysis

Local Sensitivity Approaches are typically based on the computation of local (i.e., corresponding to a specific location in the parameter space) derivatives of the model output with respect to parameter values. To reveal how the sensitivity of a model output varies across the parameter space, Rakovec et al. (2014) suggest performing a Distributed Evaluation of Local Sensitivity Analysis (*DELSA*). The latter essentially consists of performing multiple evaluations of LSA across the parameter space to evaluate the local sensitivity indices S_{L_i} for each uncertain parameter as follows:

$$\begin{cases} S_{L_i}^j = \frac{\left(\frac{\partial u_e}{\partial \lambda_i} \Big|_{p^j}\right)^2 V[\lambda_i]}{V_L^j(u_e)} & , \quad 1 \leq i \leq 3 \\ V_L^j(u_e) = \sum_{i=1}^3 \left(\frac{\partial u_e}{\partial \lambda_i} \Big|_{p^j}\right)^2 V[\lambda_i], \end{cases} \quad (8)$$

where $V[\cdot]$ refers to variance and p^j refers to the grid structure nodes of the uniformly partitioned three-dimensional parameter support λ_u (i.e., the uncertain parameters space), partial derivatives $\left(\frac{\partial u_e}{\partial \lambda_i}\right)$ being evaluated at such nodes. Here, each parameter support λ_i is partitioned into 100 intervals. Thus, we employ 1 million points in the parameter space considering the above mentioned three uncertain parameters (i.e., $j = 1, 2, \dots, 1 \times 10^6$).

Figure 9 depicts sensitivity maps (in terms of mean and standard deviation) of local sensitivity indices S_{L_i} as a function of model parameter values, for 5 time steps. Figure 9 allows identifying regions of the parameter space characterized by diverse responses to input parameter variability. Notably, effluent concentration, u_e , displays similar sensitivity patterns to K_l and Q , these two parameters likely having complementary effects on solute breakthrough times (see also Figure 7c). Overall, the importance of Pe is smaller if compared with the sorption parameters, this result being consistent with the GSA results (see Figure 8). However, we observe that local sensitivities to Pe generally tends to increase for $Pe > 55$. We recall that the mesh-free partial derivatives of solute concentrations at the system outlet (u_e) with respect to the parameters are inferred almost instantly as a direct post-processing of our PINN-UU. The terms $\frac{\partial u_e}{\partial \lambda_i}$ appearing in (8) can then be computed without having to replace these derivatives with incremental ratios, as routinely done when employing standard numerical solvers. The PINN-UU neural

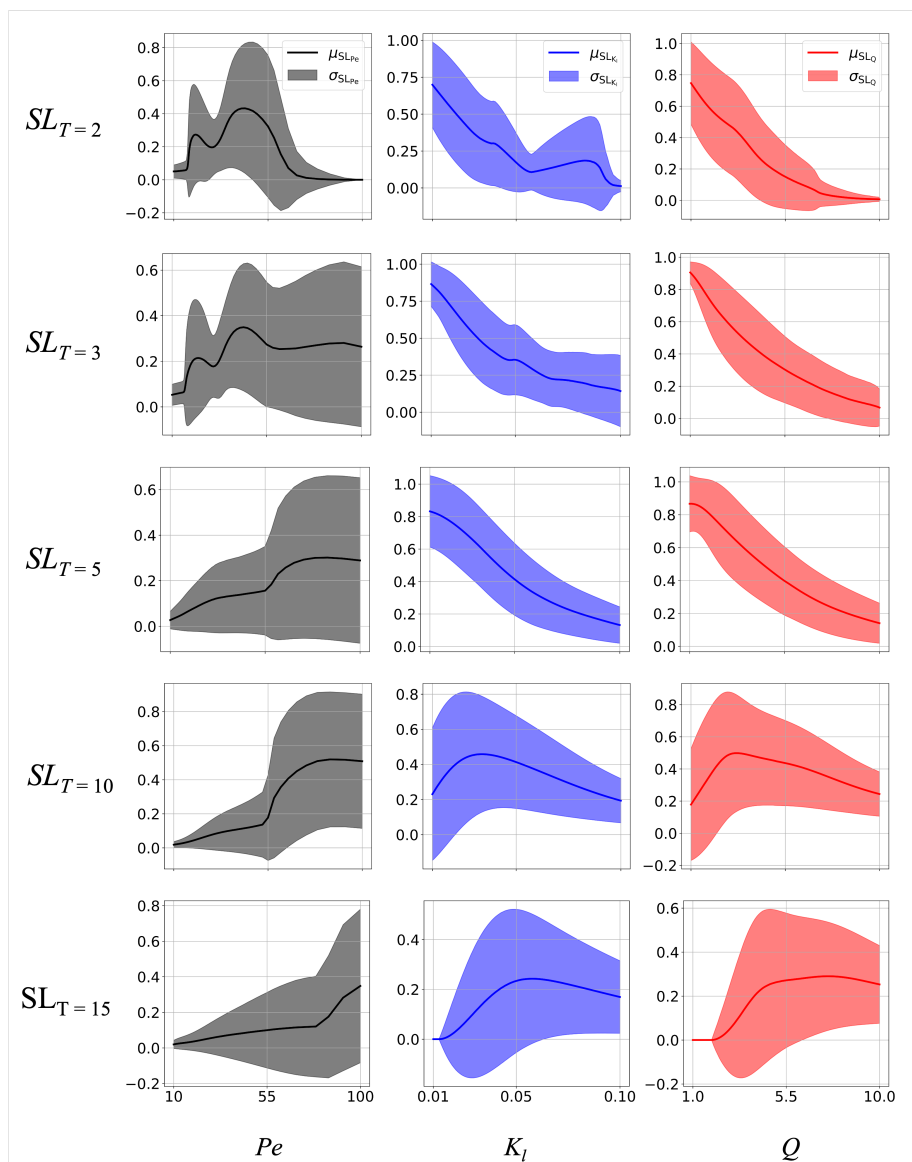


Fig. 9: Local Sensitivity Indices. Variability of first two statistical moments of local sensitivity indices (mean μ_{SL_λ} , and standard deviation σ_{SL_λ}) with model parameters, i.e., Péclet number (Pe ; in black), Adsorption rate (K_l ; in blue), and Maximum adsorption (Q ; in red) as calculated through Distributed Evaluation of Local Sensitivity Analysis (DESLA) at the outlet section of the system for times $T = \{2, 3, 5, 10, 15\}$.

network allows computation of such gradient through automatic differentiation, the same approach employed for spatial and temporal derivatives.

5 Conclusions

We develop a physics-informed neural network under uncertainty (PINN-UU) to bridge between physics-informed optimization and uncertainty quantification. We show how our PINN-UU based neural solver can take uncertain PDE parameters as input to its fully physics-driven network. Key conclusions stemming from results are listed in the following.

1. Our work documents how to embed the multi-dimensional space associated with uncertain parameters of a PDE taken to describe the dynamics of a physical system within the conceptual and operational framework associated with PINNs. We introduce a step-wise training procedure upon leveraging on transfer learning (warm-starting) techniques (Sections 3.1 and 4.1.2). The procedure enables us to:
 - (a) alleviate the complexities related to the tuning of the parameters of the neural solver in high-dimensional problems, where the choice of the prior distributions for the physical and neural network parameters does not have a significant impact on the approximation performance anymore,
 - (b) ease computational costs of the training process by an optimum initialization technique.
2. We rely on unsupervised learning to infer the solution over multiple instances of a parametric nonlinear PDE. Our numerical results are related to a transport scenario featuring advection-dispersion coupled with nonlinear sorption and closely correspond to conditions documented in laboratory scale column experiments. When compared to a benchmark numerical solution, as rendered through a traditional Finite Difference solution of the governing PDE, PINN-UU results have acceptable generalization errors even in advection dominated cases.
3. We test the capability of PINN-UU in accurately propagating uncertainty from input parameters to model outputs, such as solute breakthrough curves. Once trained, PINN-UU can yield probability distributions of target model outputs through inexpensive sampling of the solution space. PINN-UU can reproduce the probability distributions of temporally varying concentrations at the system outlet with high degree of fidelity when compared with the results of a standard Monte Carlo simulation performed through the benchmark Finite Difference solution. The model is capable of accurately evaluating markedly skewed probability distributions of solute concentrations featuring marked changes in their shape along time.
4. Outputs of PINN-UU are amenable to be readily employed in the context of global and local sensitivity analysis. After training, the model can provide solution maps as a function of space, time, and parameters at negligible additional computational cost. These can then be readily exploited to evaluate sensitivity metrics, such as moment-based global sensitivity indices (Section 4.3.1) or

the DELSA indicators (Section 4.3.2). Our proposed method can then assist to appropriately design the parametric search space in field/laboratory scale sampling campaigns.

Our approach shows promising potential in addressing high dimensional transient linear/non-linear PDEs. Most of the modifications of vanilla PINNs, such as, for example, bounded residual-based attention (RBA) (Anagnostopoulos et al., 2023), locally adaptive activation functions (Jagtap et al., 2020), and gradient enhanced PINNs (Yu et al., 2022), to name but a few, can be implemented within the PINN-UU framework. In this context, addressing solute transport within randomly heterogeneous porous media represents a clear future direction for further developments of PINN-UU.

Declarations

Funding. The authors acknowledge financial support from the European Union’s Horizon 2020 research and innovation programme under the Marie Skłodowska-Curie grant agreement No 956384

Code availability. Codes used in this paper will be available in the following github repository <https://miladpnh.github.io>

References

- Anagnostopoulos SJ, Toscano JD, Stergiopoulos N, Karniadakis GE (2023) Residual-based attention and connection to information bottleneck theory in pinns. arXiv preprint arXiv:230700379
- Asher MJ, Croke BF, Jakeman AJ, Peeters LJ (2015) A review of surrogate models and their application to groundwater modeling. *Water Resources Research* 51(8):5957–5973
- Ballio F, Guadagnini A (2004) Convergence assessment of numerical monte carlo simulations in groundwater hydrology. *Water resources research* 40(4)
- Barron AR (1993) Universal approximation bounds for superpositions of a sigmoidal function. *IEEE Transactions on Information theory* 39(3):930–945
- Bethke CM (2022) *Geochemical and biogeochemical reaction modeling*. Cambridge university press
- Blechsmidt J, Ernst OG (2021) Three ways to solve partial differential equations with neural networks — a review. *GAMM-Mitteilungen* 44(2):e202100,006, DOI <https://doi.org/10.1002/gamm.202100006>, URL <https://onlinelibrary.wiley.com/doi/abs/10.1002/gamm.202100006>
- Carrera J, Neuman SP (1986) Estimation of aquifer parameters under transient and steady state conditions: 2. uniqueness, stability, and solution algorithms. *Water Resources Research* 22(2):211–227
- Cerretti G, Guadagnini L, Porta G, Guadagnini A (2018) Local and global sensitivity analysis of cr (vi) geogenic leakage under uncertain environmental conditions. *Water Resources Research* 54(8):5785–5802

- Condon LE, Kollet S, Bierkens MF, Fogg GE, Maxwell RM, Hill MC, Fransen HJH, Verhoef A, Van Loon AF, Sulis M, et al. (2021) Global groundwater modeling and monitoring: Opportunities and challenges. *Water Resources Research* 57(12):e2020WR029,500
- Crawford J (1999) Geochemical modelling—a review of current capabilities and future directions
- Cybenko G (1989) Approximation by superpositions of a sigmoidal function. *Mathematics of control, signals and systems* 2(4):303–314
- Dai Z, Samper J (2004) Inverse problem of multicomponent reactive chemical transport in porous media: Formulation and applications. *Water Resources Research* 40(7)
- Dell’Oca A, Riva M, Guadagnini A (2017) Moment-based metrics for global sensitivity analysis of hydrological systems. *Hydrology and Earth System Sciences* 21(12):6219–6234, DOI 10.5194/hess-21-6219-2017
- Fajraoui N, Ramasomanana F, Younes A, Mara TA, Ackerer P, Guadagnini A (2011) Use of global sensitivity analysis and polynomial chaos expansion for interpretation of nonreactive transport experiments in laboratory-scale porous media. *Water Resources Research* 47(2)
- Fetter CW, Boving TB, Kreamer DK (1999) Contaminant hydrogeology, vol 1138. Prentice hall Upper Saddle River, NJ
- Glorot X, Bengio Y (2010) Understanding the difficulty of training deep feedforward neural networks. In: *Proceedings of the thirteenth international conference on artificial intelligence and statistics, JMLR Workshop and Conference Proceedings*, pp 249–256
- He J, Sætrom J, Durlafsky LJ (2011) Enhanced linearized reduced-order models for subsurface flow simulation. *Journal of Computational Physics* 230(23):8313–8341
- He Q, Tartakovsky AM (2021) Physics-informed neural network method for forward and backward advection-dispersion equations. *Water Resources Research* 57(7):e2020WR029,479
- Jagtap AD, Kawaguchi K, Em Karniadakis G (2020) Locally adaptive activation functions with slope recovery for deep and physics-informed neural networks. *Proceedings of the Royal Society A* 476(2239):20200,334
- Janetti EB, Riva M, Guadagnini A (2021) Natural springs protection and probabilistic risk assessment under uncertain conditions. *Science of the Total Environment* 751:141,430
- Kingma DP, Ba J (2014) Adam: A method for stochastic optimization. *arXiv preprint arXiv:1412.6980*
- Kingma DP, Ba J, Bengio Y, LeCun Y (2015) 3rd international conference on learning representations. ICLR, San Diego
- Lagaris IE, Likas A, Fotiadis DI (1998) Artificial neural networks for solving ordinary and partial differential equations. *IEEE transactions on neural networks* 9(5):987–1000
- Lagaris IE, Likas AC, Papageorgiou DG (2000) Neural-network methods for boundary value problems with irregular boundaries. *IEEE Transactions on Neural Networks* 11(5):1041–1049
- Le Maître O, Knio OM (2010) Spectral methods for uncertainty quantification: with applications to computational fluid dynamics. Springer Science & Business Media

- LeCun Y, Bengio Y, Hinton G (2015) Deep learning. *nature* 521(7553):436–444
- Lee SH, Chen W (2009) A comparative study of uncertainty propagation methods for black-box-type problems. *Structural and multidisciplinary optimization* 37:239–253
- Liu DC, Nocedal J (1989) On the limited memory bfgs method for large scale optimization. *Mathematical programming* 45(1-3):503–528
- Liu Y, Durlflosky LJ (2021) 3d cnn-pca: A deep-learning-based parameterization for complex geomodels. *Computers & Geosciences* 148:104,676
- Lye KO, Mishra S, Ray D, Chandrashekar P (2021) Iterative surrogate model optimization (ismo): An active learning algorithm for pde constrained optimization with deep neural networks. *Computer Methods in Applied Mechanics and Engineering* 374:113,575
- Manzoni A, Porta GM, Guadagnini L, Guadagnini A, Riva M (2023) Probabilistic reconstruction via machine-learning of the po watershed aquifer system (italy). *Hydrogeology Journal* 31(6):1547–1563
- McClenny L, Braga-Neto U (2020) Self-adaptive physics-informed neural networks using a soft attention mechanism. *arXiv preprint arXiv:200904544*
- Mishra S (2018) A machine learning framework for data driven acceleration of computations of differential equations. *arXiv preprint arXiv:180709519*
- Mishra S, Molinaro R (2022) Estimates on the generalization error of physics-informed neural networks for approximating a class of inverse problems for pdes. *IMA Journal of Numerical Analysis* 42(2):981–1022
- Mishra S, Molinaro R (2023) Estimates on the generalization error of physics-informed neural networks for approximating pdes. *IMA Journal of Numerical Analysis* 43(1):1–43
- Neuman SP (2003) Maximum likelihood bayesian averaging of uncertain model predictions. *Stochastic Environmental Research and Risk Assessment* 17(5):291–305
- Nwankpa C, Ijomah W, Gachagan A, Marshall S (2018) Activation functions: Comparison of trends in practice and research for deep learning. *arXiv preprint arXiv:181103378*
- Panzeri M, Riva M, Guadagnini A, Neuman SP (2014) Comparison of ensemble kalman filter groundwater-data assimilation methods based on stochastic moment equations and monte carlo simulation. *Advances in Water Resources* 66:8–18
- Pasetto D, Guadagnini A, Putti M (2011) Pod-based monte carlo approach for the solution of regional scale groundwater flow driven by randomly distributed recharge. *Advances in water resources* 34(11):1450–1463
- Pasetto D, Guadagnini A, Putti M (2014) A reduced-order model for monte carlo simulations of stochastic groundwater flow. *Computational Geosciences* 18:157–169
- Psaros AF, Meng X, Zou Z, Guo L, Karniadakis GE (2023) Uncertainty quantification in scientific machine learning: Methods, metrics, and comparisons. *Journal of Computational Physics* 477:111,902
- Raissi M (2023) Open problems in applied deep learning. *arXiv preprint arXiv:230111316*
- Raissi M, Karniadakis GE (2018) Hidden physics models: Machine learning of non-linear partial differential equations. *Journal of Computational Physics* 357:125–141

- Raissi M, Perdikaris P, Karniadakis GE (2017) Physics informed deep learning (part i): Data-driven solutions of nonlinear partial differential equations. arXiv preprint arXiv:171110561
- Raissi M, Perdikaris P, Karniadakis GE (2019) Physics-informed neural networks: A deep learning framework for solving forward and inverse problems involving nonlinear partial differential equations. *Journal of Computational physics* 378:686–707
- Raissi M, Yazdani A, Karniadakis GE (2020) Hidden fluid mechanics: Learning velocity and pressure fields from flow visualizations. *Science* 367(6481):1026–1030
- Rakovec O, Hill MC, Clark M, Weerts A, Teuling A, Uijlenhoet R (2014) Distributed evaluation of local sensitivity analysis (delsa), with application to hydrologic models. *Water Resources Research* 50(1):409–426
- Ray D, Hesthaven JS (2018) An artificial neural network as a troubled-cell indicator. *Journal of computational physics* 367:166–191
- Riva M, Guadagnini A, Dell’Oca A (2015) Probabilistic assessment of seawater intrusion under multiple sources of uncertainty. *Advances in Water Resources* 75:93–104
- Shen C, Appling AP, Gentine P, Bandai T, Gupta H, Tartakovsky A, Baity-Jesi M, Fenicia F, Kifer D, Li L, et al. (2023) Differentiable modeling to unify machine learning and physical models and advance geosciences. arXiv preprint arXiv:230104027
- Sobol’ I (1993) Sensitivity estimates for nonlinear mathematical models. *Math Model Comput Exp* 1:407
- Tang M, Liu Y, Durlofsky LJ (2020) A deep-learning-based surrogate model for data assimilation in dynamic subsurface flow problems. *Journal of Computational Physics* 413:109,456
- Tang M, Liu Y, Durlofsky LJ (2021) Deep-learning-based surrogate flow modeling and geological parameterization for data assimilation in 3d subsurface flow. *Computer Methods in Applied Mechanics and Engineering* 376:113,636
- Tartakovsky DM (2013) Assessment and management of risk in subsurface hydrology: A review and perspective. *Advances in Water Resources* 51:247–260
- Tipireddy R, Perdikaris P, Stinis P, Tartakovsky AM (2022) Multistep and continuous physics-informed neural network methods for learning governing equations and constitutive relations. *Journal of Machine Learning for Modeling and Computing* 3(2)
- Turnquist B, Owkes M (2019) multiuq: An intrusive uncertainty quantification tool for gas-liquid multiphase flows. *Journal of Computational Physics* 399:108,951
- Yang L, Meng X, Karniadakis GE (2021) B-pinns: Bayesian physics-informed neural networks for forward and inverse pde problems with noisy data. *Journal of Computational Physics* 425:109,913
- Yeung YH, Barajas-Solano DA, Tartakovsky AM (2022) Physics-informed machine learning method for large-scale data assimilation problems. *Water Resources Research* 58(5):e2021WR031,023
- Yu J, Lu L, Meng X, Karniadakis GE (2022) Gradient-enhanced physics-informed neural networks for forward and inverse pde problems. *Computer Methods in Applied Mechanics and Engineering* 393:114,823
- Zou Z, Karniadakis GE (2023) L-hydra: multi-head physics-informed neural networks. arXiv preprint arXiv:230102152